Crowding Induces Differences in the Diffusion of Thermophilic and Mesophilic Proteins: A New Look at Neutron Scattering Results

Enrique Marcos, Pau Mestres, and Ramon Crehuet*
Department of Biological Chemistry and Molecular Modeling, Institute of Advanced Chemistry of Catalonia (IQAC – CSIC), Barcelona, Spain

ABSTRACT The dynamical basis underlying the increased thermal stability of thermophilic proteins remains uncertain. Here, we challenge the new paradigm established by neutron scattering experiments in solution, in which the adaptation of thermophilic proteins to high temperatures lies in the lower sensitivity of their flexibility to temperature changes. By means of a combination of molecular dynamics and Brownian dynamics simulations, we report a reinterpretation of those experiments and show evidence that under crowding conditions, such as in vivo, thermophilic and homolog mesophilic proteins have diffusional properties with different thermal behavior.

INTRODUCTION

Thermophilic organisms require very high temperatures for surviving, and elucidating the adaptation strategies of their proteins can provide clues for designing new proteins with enhanced thermostability (1). This also provides novel opportunities to understand how protein sequence and structure are related with dynamics and function. To this aim, comparative studies of thermophilic proteins and their corresponding homologs working at low temperature, i.e., mesophilic, find great usefulness. There has been a long-standing controversy on the dynamical requirements for thermostability because different techniques are sensitive to dynamical processes at vastly different timescales (2–7). A few years ago, an innovative mechanism of protein thermostability was invoked by Zaccai and co-workers (8) based on elastic incoherent neutron scattering (EINS) experiments in solution. They suggested that the key dynamical feature required for protein thermostability was an enhanced resilience ($\langle k' \rangle$), which is defined as the inverse of the variation of the mean-square fluctuation ($\langle u^2 \rangle$) with temperature (9): $\langle k' \rangle = 1/(d\langle u^2 \rangle/dT)$. The smaller the temperature dependence of $\langle u^2 \rangle$ the higher the resilience. These experiments showed that, at the ~100 ps timescale, a thermophilic enzyme (Malate Dehydrogenase from *Methanococcus jannaschii*; *Mj*MalDH) was ~10 times more resilient than a mesophilic homolog (Lactate Dehydrogenase from *Oryctolagus cunniculus*; *Oc*LDH) (see *open symbols* in Fig. 1 *A*). In other words, the flexibility ($\langle u^2 \rangle$) of the thermophilic enzyme is less sensitive to temperature than that of the mesophilic one. They also observed that $\langle u^2 \rangle$ values of *Mj*MalDH were higher than those of *Oc*LDH in the temperature range studied (280–320 K), which ultimately means that higher resilience need not imply less flexibility. On the contrary, this new paradigm claims that thermoenzymes are more flexible even at low temperatures.

The correlation between resilience and thermostability has also been observed by neutron scattering experiments on whole cells from organisms adapted to different temperatures (10). Given that resilience has also been observed to be a property very sensitive to the solvent conditions (11), we question whether the higher resilience observed for thermophilic proteins arises only from protein internal dynamics, an issue that has not been addressed hitherto. In this work, we investigate the contributions from intramolecular motions and protein diffusion to the global dynamics of *Mj*MalDH and *Oc*LDH, as measured by EINS (8). We use molecular dynamics (MD) and Brownian dynamics (BD) simulations of the crowded solution (200 mg/mL) used in the experiment, which also mimics in vivo conditions. To our knowledge, this combination of MD and BD represents a new approach to incorporate crowding effects in the simulation of protein global dynamics in solution as explored by neutron scattering.

MD simulations have proven to be a valuable computational technique for exploring protein internal dynamics and are very suitable for examining neutron scattering data (12–17). MD can describe dynamical events at the short timescales (from picoseconds to hundreds of nanoseconds) that are usually explored by neutron scattering instruments. However, describing protein diffusion in solution with MD, taking into account interactions among diffusing proteins, is computationally unattainable. In contrast, BD simulations are well suited to explore translational and rotational diffusion and the interactions among hundreds of protein molecules at timescales from nanoseconds to milliseconds (18–20). Because one of the main assumptions of BD is ignoring protein internal dynamics, a combination of MD and BD simulations is promising in giving a global picture of protein dynamics in solution.

EINS experiments probe atomic motions within a space-time window defined by the characteristics of the

Submitted August 12, 2011, and accepted for publication September 23, 2011.

*Correspondence: ramon.crehuet@iqac.csic.es

Editor: Martin Blackledge.

0006-3495/11/12/2782/8 $2.00

doi: 10.1016/j.bpj.2011.09.033

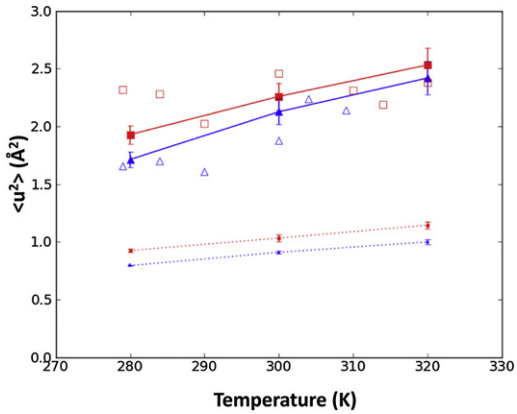

FIGURE 1 Experiment versus simulation. Comparison between experimental (8) and simulated $\langle u^2 \rangle$ values of the thermophilic (*red squares*) and mesophilic (*blue triangles*) proteins at the three temperatures studied. Simulated $\langle u^2 \rangle$ from intramolecular dynamics are represented with dashed lines, and $\langle u^2 \rangle$ including translational and rotational diffusion are represented with solid lines.

spectrometer and, in general, can cover motions of a few angstroms in hundreds of picoseconds (21). These experiments allow obtaining a measure of the average dynamics of a protein expressed as the atomic mean-square displacement (MSD) ($\langle u^2 \rangle$). To study the dynamics of a protein close to physiological conditions, these experiments are carried out in solution. This is a challenge when examining protein internal dynamics because contamination of the elastic scattering due to protein diffusion can be present (22–24) and, thus, specific sample conditions and instrumental settings are required to minimize this contribution. Because EINS experiments require high protein concentrations to be conducted satisfactorily (typically ~100–200 mg/mL), protein diffusion is hindered by such a crowded media, so that in many cases the diffusion contribution is assumed to be negligible. Furthermore, when comparing the dynamics of different proteins with similar size, it is usual practice to consider that their small diffusion is very similar and, hence, differences obtained in $\langle u^2 \rangle$ must account for differences in their intramolecular dynamics (25). Indeed, this was one of the implicit assumptions of Zaccai and co-workers (8). In this investigation we challenge this view by means of MD and BD simulations and show that a) the internal dynamics and diffusion both have similar contributions to the global flexibility measured for *Mj*MalDH and *Oc*LDH and that b) the diffusional properties of both proteins are strikingly different under crowding conditions explaining the distinct thermal behavior observed in the experiment.

MD and BD simulations were conducted at 280, 300, and 320 K spanning the range of temperatures experimentally studied. The crystal structures of both tetrameric proteins (PDB codes 1HYG (26) and 9LDT (27)) were used as inputs of the simulations. MD simulations were performed with Gromacs (28). Each MD simulation was equilibrated for 40 ns and a production run of 160 ns followed. To have an estimate of our error and to probe potentially different conformations, we have used five points of these long trajectories to simulate the EINS data, as further explained in the Supporting Material. BD simulations were carried out with the code developed by Elcock and co-workers (18,19). BD simulations of each protein were conducted under periodic boundary conditions in a 1000-molecule box with the same experimental concentration (200 mg/mL). The sensitivity of the results to BD parameters has also been considered (see the Supporting Material). We have generated time-trajectories (hereafter called MD+BD) composed of intramolecular motions from MD simulations and both translational and rotational diffusive motions from BD simulations. Comparison with experiment is possible by calculating the MSD ($\langle u^2 \rangle$) from computational results using the same data treatment methods as in the experiment (29). This implies calculating from the MD and MD+BD trajectories the basic quantity measured in neutron scattering, the scattering function $S(Q, \omega = 0)$, and including the effects of the energy resolution and Q-range of the experiment. The $\langle u^2 \rangle$ is obtained using the Gaussian approximation (see Materials and Methods and Supporting Material for details of the simulation protocols and analysis).

MATERIALS AND METHODS

Elastic incoherent neutron scattering

Neutron scattering experiments obtain information of the atomic motions in a sample by measuring the exchange of momentum (Q) and energy (ω) of the incident neutrons in a scattering process (21). The basic quantity obtained from these experiments that contains information on the dynamics of the sample is the dynamic structure factor $S(Q, \omega)$. The contribution from nonhydrogen atoms to incoherent scattering is negligible, given their much smaller scattering length. Because hydrogens are homogeneously distributed throughout a protein structure, the observed structure factor gives an average measure of the dynamics of the sample.

The energies of incident neutrons are described by the energy resolution function, $R(\omega)$, which depends on the neutron spectrometer. The width of $R(\omega)$ determines the timescale of motions accessible by the instrument, with narrower widths corresponding to longer timescales. The momentum transfer, on the other hand, defines the spatial scale of motions accessible by the instrument. Therefore, $S(Q, \omega)$ gives information on the dynamics of the sample within a well-defined space-time window of observation. The EINS experiments in (8) were done on the IN13 instrument at ILL (Grenoble, France), which has an energy resolution of 8 μeV (full width at half-maximum). The Q-range used was 1.2–2.2 $Å^{-1}$. These experimental conditions have access to motions of ~1 Å in ~100 ps.

The elastic peak corresponds to the structure factor measured without exchange of energy, $S(Q, \omega = 0)$. We employed the Gaussian approximation for extracting the MSD of the sample. The elastic intensity is Q dependent and for confined motions takes the following form:

$$S(Q, \omega = 0) = e^{-\frac{1}{6}\langle u^2 \rangle Q^2}, \quad (1)$$

where $\langle u^2 \rangle$ is the MSD averaged over the atoms in the protein. Linearization of Eq. 1 by taking the slope of a natural log plot of $S(Q, \omega = 0)$ vs. Q^2 (Guinier plot) allows obtaining $\langle u^2 \rangle$.

Following Hayward and Smith (29), for a quantitative comparison between simulated trajectories and the experimental MSDs we computed the dynamic structure factor and then extracted the MSD with Eq.1. To compute S(Q, $\omega = 0$), we first need to calculate $F_{inc}(Q, t)$ in the Q range studied experimentally using Eq. 2:

$$F_{inc}(Q,\ t)\ =\ \frac{1}{N}\sum_{\alpha} b^2_{\alpha,\ inc}\left\langle e^{i\mathbf{q}(\mathbf{R}(t)-\mathbf{R}(0))}\right\rangle. \qquad (2)$$

For each experimental Q value, $F_{inc}(Q, t)$ is an average over a number of q vectors with random orientations and the same modulus $Q = |\mathbf{q}|$. In this work, we have averaged $F_{inc}(Q, t)$ with 50 $\mathbf{q}$ vectors to guarantee an isotropic distribution of $\mathbf{q}$ vectors. We finally compute the convoluted structure factor by Fourier transforming the product $F_{inc}(Q, t)\cdot R(t)$, where R(t) is the Fourier transform of the energy resolution function $R(\omega)$, described as a Lorentzian. The analysis of simulated trajectories to obtain neutron scattering properties has been performed with the nMoldyn program (30).

Molecular dynamics

All MD simulations were performed with the GROMACS 4.0.5 package (28). Each simulated system consisted of a single tetrameric protein immersed in a rhombic dodecahedral water box with Na^+ and Cl^- ions that were added for neutrality. Standard protonation states were assigned to all protein residues. In agreement with the experiment, substrates bound to the crystallographic structures were removed. The total numbers of atoms in the simulations of the thermophilic and mesophilic proteins are 89,229 and 90,393, respectively.

The two systems under study were subjected to ~200 ns simulations at 280, 300, and 320 K at constant temperature and pressure. The temperature was kept constant with the Berendsen thermostat (31) with a coupling time constant of 0.1 ps. The pressure was controlled with the Berendsen barostat (31) with a coupling constant of 0.5 ps and an isotropic compressibility of $4.5\cdot10^{-5}$ bar^{-1}. The OPLS all-atom (32) force field was used in combination with the TIP3P model (33) for water molecules. Periodic boundary conditions were used. Short-range electrostatic interactions were calculated explicitly with a 10 Å cutoff and long-range electrostatic interactions were calculated with the particle mesh Ewald method (34) with a grid spacing of 1.2 Å and a fourth-order spline interpolation. Lennard-Jones interactions were calculated using a switch function between 0.8 and 0.9 nm. All bonds were constrained using the LINCS algorithm (35), which allowed using an integration time step of 2 fs.

Each MD simulation was setup as follows. The structure of the solvated protein was energy minimized with the steepest descent algorithm. Next, to equilibrate the solvent surrounding the protein an MD simulation at the target temperature was performed with harmonic position restraints on the heavy atoms of the protein with a force constant of 1000 kJ mol^{-1} nm^{-2}. Subsequently, a 200 ns trajectory was carried out and the last 160 ns were used for production. We have performed simulations with two aims. First, we ran long trajectories (~200 ns and saved each 20 ps) to have access to different conformations. Second, we have run five short trajectories (2 ns length and saved each 1 ps) starting from different regions of the potential energy surface explored by the long MD trajectories (at 10, 50, 100, and 160 ns after the 40 ns of equilibration). The aim of these short trajectories is to assess the conformational dependence of intramolecular motions at the 100 ps timescale probed by neutron scattering. To analyze the contribution of intramolecular dynamics to $\langle u^2\rangle$ we have subtracted translations and rotations by superimposing each frame to a reference structure.

Brownian dynamics

We have followed the same setup as Elcock and co-workers (19) (see the Supporting Material for details). BD simulations for each protein were conducted for 10 μs at 280, 300, and 320 K under periodic boundary conditions in a cubic cell of 1000 molecules. The simulations were equilibrated for 2 μs and the last 8 μs were used for production. A time step of 2.5 ps was used for all simulations. The production runs of 8 μs were used for computing radial distribution functions. In addition, after the 2 μs of equilibration another production run of 2 ns with a shorter time step (1 ps) was followed for each protein at each temperature to describe the diffusive motion at the experimental timescale of 100 ps with better resolution. These 2 ns trajectories were used to generate MD+BD trajectories (see below) for computing neutron scattering properties.

The translational diffusion coefficient (self-diffusion) was calculated from the Einstein relation $D_{trans}(\Delta t) = MSD/(6\Delta t)$, where MSD is computed as

$$MSD(\Delta t)\ =\ \frac{1}{N(T-\Delta t+1)}\sum_{t}^{N}\sum_{t=0}^{T-\Delta t}\left[R_i(t+\Delta t)-R_i(t)\right]^2, \qquad (3)$$

where MSD is averaged over N atoms, T is the time length of the trajectory, and Δt the time separation between saved frames.

Generation of MD+BD trajectories

To describe the global dynamics of a protein molecule we have treated the intramolecular protein motions decoupled from rigid-body diffusive motions (translations and rotations), a realistic assumption as shown in (36). We have generated a trajectory composed by intramolecular motions described by MD simulations (after subtraction of translations and rotations) and diffusive motions obtained from BD simulations. Herein this trajectory will be referred as MD+BD trajectory and is generated as

$$\mathbf{r}^m(t)\ =\ \mathbf{r}_{MD}(t)\cdot\mathbf{R}^m_{rot}(t)+\mathbf{R}^m_{cm}(t) \qquad (4)$$

where $\mathbf{r}^m(t)$ and $\mathbf{r}_{MD}$ (t) are the 3N-dimensional vectors of atomic coordinates of the MD+BD trajectory for molecule m and the MD trajectory respectively, $\mathbf{R}^m_{rot}(t)$ is the 3×3 rotational matrix of molecule m at time t and $\mathbf{R}^m_{cm}(t)$ is the time-dependent position of the center of mass of molecule m.

We have generated 60 MD+BD trajectories from 60 randomly chosen molecules from the 1000-molecule box to compute $\langle u^2\rangle$ at each temperature. We have proven that the obtained $\langle u^2\rangle$ is well converged with 60 random molecules. Because of the negligible conformational dependence of the short time MD trajectories, we have used the same MD trajectory to build each MD+BD trajectory. Therefore, the difference between these 60 trajectories will come from differences in the rotational and translational diffusive motions of each molecule. Subsequently, S(Q, $\omega = 0$) was calculated for each molecule and averaged for all molecules at each Q value. A Guinier plot of these averaged S(Q) values was done for extracting the $\langle u^2\rangle$ of the crowded solution.

Figures including molecular structures and electrostatic potentials have been generated using VMD (37) and APBS (38,39). The structural alignments have been performed with DALI (40).

RESULTS AND DISCUSSION

Intramolecular dynamics

The simulated $\langle u^2\rangle$ obtained from the MD simulations (*dashed lines* in Fig. 1) are qualitatively consistent with the experiment (8) in that the thermophilic protein is more flexible than the mesophilic one, but they are underestimated by ~1$Å^2$ with respect to the experiment (8). The thermophilic protein has higher flexibility both in the backbone

(Fig. 2) and in all residue atoms (Fig. S1 in the Supporting Material). We have quantified the temperature dependence of $\langle u^2 \rangle$ with the slope of a linear fit of $\langle u^2 \rangle$ versus temperature, $d\langle u^2 \rangle/dT$, and noted that it is the same for both proteins (0.005 $Å^2\ K^{-1}$). This is also in contrast to the experiment (8) where $d\langle u^2 \rangle/dT$ was observed to be much lower for the thermophilic protein (0.002 vs. 0.020 $Å^2\ K^{-1}$). We have checked that the conformational dependence of intramolecular $\langle u^2 \rangle$ is negligible (see *small error bars in dashed lines* from Fig. 1). The significant difference between simulated and experimental $\langle u^2 \rangle$ values indicate that, in the experiment, the apparent $\langle u^2 \rangle$ values not only correspond to internal protein dynamics and that an important contribution from translational and rotational diffusion must be present. This is also supported by former MD studies that have been successful in reproducing neutron scattering data from a wide range of biological systems where protein diffusion was absent, i.e., protein powders (12–15) and membrane proteins (16,17).

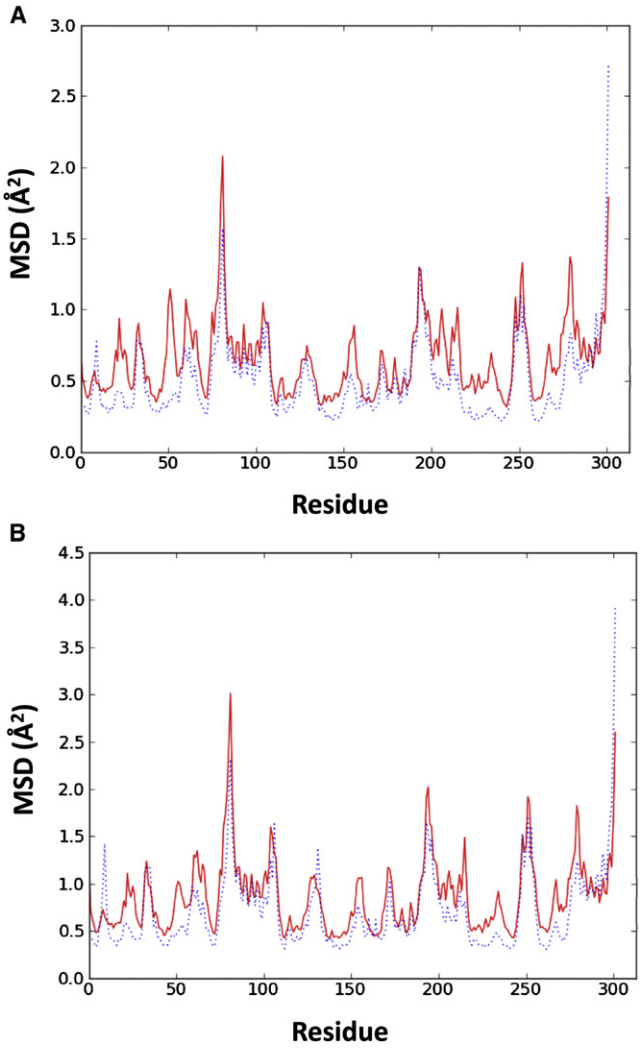

FIGURE 2 Thermophilic enzyme is more flexible in almost all regions. Representation of the MSD of the backbone atoms of the thermophilic (*red*) and mesophilic (*blue*) proteins residues at (*A*) 280 K and (*B*) 320 K. and is averaged over the four chains. For better comparison, the residues of both proteins have been structurally aligned. Remark that flexible regions are correlated between both proteins. The higher mobility of the thermophile is distributed throughout all the residues, and is not the result of a particularly flexible region. When all the atoms of the residue are included, higher fluctuations are observed but the trend does not change (see Fig. S1).

Macromolecular diffusion in the crowded media

Now we turn our attention to the contribution from diffusion to the measured $\langle u^2 \rangle$. A snapshot of a BD simulation of the-crowded solution (thermophilic enzyme at 280 K) is shown in Fig. 3 *A*. Fig. 1 shows the $\langle u^2 \rangle$ values obtained from MD+BD trajectories (see *solid lines*). The agreement between the simulated and experimental $\langle u^2 \rangle$ values has been significantly improved. Both translational and

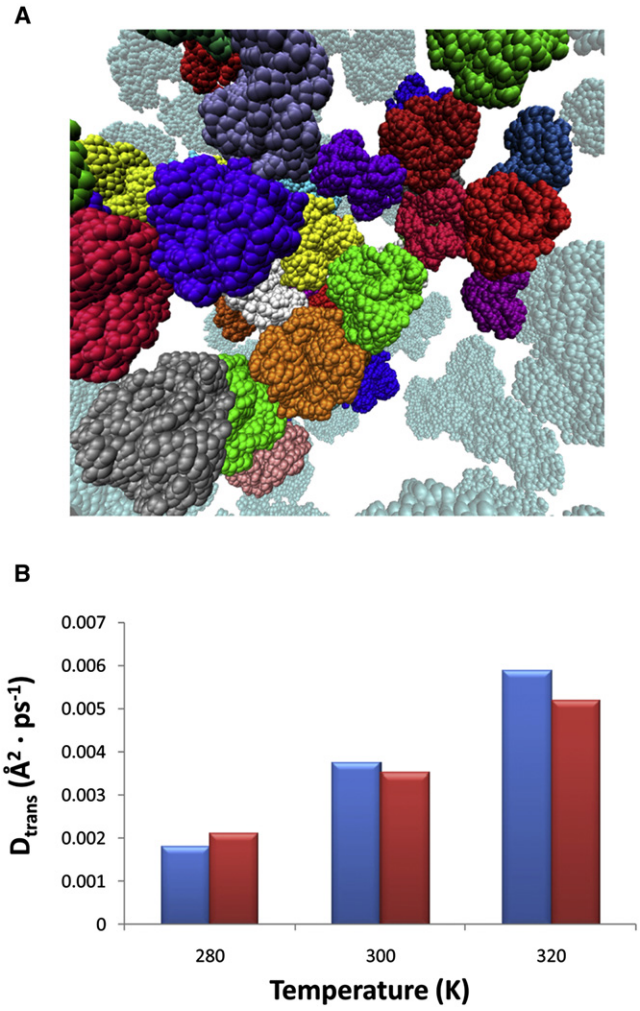

FIGURE 3 Diffusion in the crowded media. (*A*) Snapshot of the thermophilic protein solution simulated with Brownian dynamics at 200 mg/mL and at 280 K. (*B*) Translational diffusion coefficients at 100 ps. Red and blue bars correspond to the thermophilic and mesophilic proteins, respectively, at the three temperatures studied.

rotational diffusion contribute to $\langle u^2 \rangle$ and their separated contributions are shown in Fig. S2. This is of the utmost importance for a correct interpretation of the experiment. From our results, both internal protein dynamics and diffusion have similar contributions to the experimental $\langle u^2 \rangle$ and, therefore, underestimating the diffusion contribution can lead to erroneous interpretation of EINS data, as noted by several authors (22–24). In that respect, we would like to underscore the importance of measurements on self-diffusion coefficients as an ideal complement of EINS experiments in solution.

The agreement between the experimental and simulated $d\langle u^2 \rangle/dT$ of the mesophilic protein is striking, being 0.020 and 0.018 $Å^2 \cdot K^{-1}$, respectively. For the thermophilic protein, the simulated $d\langle u^2 \rangle dT$ (0.015 $Å^2\ K^{-1}$) is lower (see also the Supporting Material) than that of the mesophilic protein, in accord with the experiment. For the thermophile we get a slightly lower $d\langle u^2 \rangle/dT$ than the mesophile. This value is still much higher than the experimental one, which suggests that we might be underestimating the difference in diffusional properties of the mesophile and the thermophile. In particular, the aggregation effects of the thermophile (vide infra) could need a better treatment than the Brownian model used. This fact, instead of invalidating our conclusions, underscores that assuming similar diffusional properties for both molecules is not correct, despite their similar size and shape.

Fig. 3 *B* shows the translational diffusion coefficient (at the experimental timescale of 100 ps) obtained from BD simulations of thermophilic and mesophilic proteins: the diffusion of the mesophilic protein is more temperature dependent than that of the thermophilic one. Because of this, the global dynamics and, thus, the $\langle u^2 \rangle$ of the thermophilic protein become less temperature-dependent than that of the mesophilic one, as pointed out above.

Interparticle interactions in the crowded media

Despite the similar weight and size of the two proteins, the different amino acid composition of their surfaces must be responsible for important differences in their diffusional properties within the crowded environment, where excluded-volume effects enhance protein-protein interactions (41). Indeed, thermophilic proteins are characterized by their higher proportion of charged residues (Asp, Glu, Lys, Arg) (42) in the surface relative to mesophilic homologs and thus electrostatic and hydrophobic protein-protein interactions are comparatively different in both proteins. Here, we explore how the amino acid composition of protein surfaces can affect the diffusional properties. Fig. 4 *A* illustrates the differences in the electrostatic potential of both proteins. The higher intensity of colors and the longer field lines in the thermophilic protein represent the stronger electrostatic interactions that are present among this type of molecules. Fig S3 plots the electrostatic energy of the six BD simulations and clearly shows that electrostatic interactions in the thermophilic protein system are notoriously more stabilizing than in the mesophilic one at the three temperatures studied. Despite the higher net charges of the thermophilic protein (−24 vs. 6 electronic units), electrostatic interactions are not necessarily repulsive, because the heterogeneous charge distribution at the surface (see Fig. 4 *A*) allows protein molecules to interact through oppositely charged protein areas by changing their relative orientations. It turns out that the increased proportion of charged residues in the thermophilic protein system results in more intense and favorable electrostatic interactions.

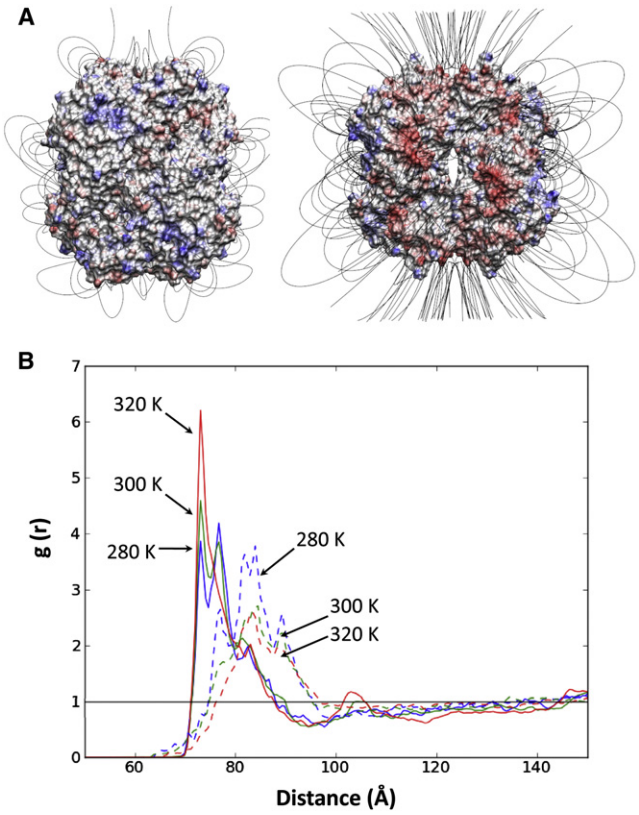

FIGURE 4 Electrostatic interactions. (*A*) Molecular structures of the mesophilic (*left*) and thermophilic (*right*) proteins colored according to the electrostatic potential at 300 K. Field lines are also represented. Blue and red colors represent areas of the protein where positive and negative charge density is accumulated. (*B*) Radial distribution functions, g(r), obtained from simulations of the thermophilic (*solid lines*) and mesophilic (*dashed lines*) proteins at 280 K (*blue*), 300 K (*green*), and 320 K (*red*).

The difference in the mutual interactions between thermophilic and mesophilic proteins is well illustrated by the radial distribution functions, g(r), obtained from BD simulations (see Fig. 4 *B*). Two remarkable differences between both proteins are observed. First, the thermophilic protein displays stronger short-range attractive interactions than the mesophilic one, as shown by higher peaks at shorter interprotein distances (both proteins have a radius of ~35 Å). Second, these short-range attractive interactions in the

thermophilic protein are enhanced upon increasing temperature, whereas in the mesophilic one they are weakened. Both features are in line with the observation in Fig. S3 that the electrostatic energy in the thermophilic protein system is lower, as pointed out previously, and that it decreases with temperature as opposed to the mesophilic protein system. Indeed, it is widely accepted that electrostatic interactions between oppositely charged protein residues increase with temperature due to a reduction of the dielectric constant of water, which ultimately leads to a reduction in the desolvation penalty required for salt bridge formation. Such enhancement of salt bridge interactions within a protein has been quantified in (43–47) and has been suggested as a key mechanism underlying the increased thermostability of thermophilic proteins, which have an increased number of charged residues (42). The thermal stabilization of electrostatic interactions in the thermophilic protein system implies that, upon increasing temperature, the interacting molecules will be closer to each other enhancing excluded volume effects and forming transient complexes that, due to their larger size, tend to diffuse at a lower rate. In view of this, the natural increase in diffusion with temperature is partially compensated by enhanced attractive interactions that increase the population of slower diffusive clusters. We suggest that this effect accounts for the differences we observe from BD in the temperature dependence of g(r) and, ultimately, in the diffusion of both proteins. Indeed, the smaller temperature dependence of the self-diffusion coefficient of the thermophilic protein can be viewed as an extension of the corresponding states model in that the thermophilic and mesophilic proteins have similar diffusional properties at their optimum temperature for activity. The implications of the enhancement of electrostatic interactions with temperature on diffusion had not been described so far. Although we already captured the main trends observed in the experiment, the different surface composition can result in other effects not taken into account by the present model. The description of the solvent as a continuum in the BD simulations oversights hydrodynamic interactions (48) and the effects of hydration water (49–51), which has been shown to play a key role in the association kinetics between proteins (52) and in protein hydrodynamics (53). In this regard, former studies (54,55) already showed that hydration water molecules of thermophilic proteins are more densely packed and exhibit less mobility than those of mesophilic homologs due to the aforementioned differences in surface composition. Therefore, hydration effects are likely to modulate the association events already observed from BD and, thus, protein diffusion. Overall, differences in interprotein interactions, hydration, and hydrodynamic interactions will largely account for the observed differences in the macromolecular motion of both enzymes.

Earlier experimental studies showed that variations in the effective charge of the bovine serum albumin, by changing the pH (56) and ionic strength (57), tune interprotein electrostatic interactions and, as a consequence, affect the diffusional behavior. This sensitivity of interprotein interactions to charge variations is fully consistent with our observation that the differences in the electrostatic properties of the thermo-mesophilic pair lead to different diffusional properties.

CONCLUSIONS

We can ultimately argue that the EINS experiment performed by Zaccai and co-workers (8), instead of revealing specific features of internal flexibility linked to thermostability, shows how a thermo-mesophilic pair of proteins can have very different diffusional properties within a crowded media, despite having strikingly similar shape and molecular weight. This illustrates the important implications of protein diffusion on the interpretation of EINS data and opens new perspectives on other previous studies in solution (10,11,25). Ultimately, this supports the idea that the concept of resilience (9) must be handled with care to characterize protein internal dynamics in solution.

Yet, no comparative studies on the diffusion of thermo-mesophilic pairs have been reported. To our knowledge, this is the first study pointing to important differences in the diffusional properties of a thermo-mesophilic pair of proteins based on theoretical and experimental data. We anticipate that this might be a general difference between thermophilic and mesophilic proteins opening up opportunities to new experimental studies. We wonder whether such difference in the thermal behavior of diffusion is linked to a requirement for maximum activity at the corresponding physiological conditions where crowding effects dominate. We leave as future work experimental studies on the diffusion of both proteins. Given the vast diversity of dynamical events at the intramolecular and diffusion level, we will also explore the dynamics of this thermo-mesophilic pair at longer timescales. This may help us to understand why the thermophilic enzyme is less active at low temperatures, though being more flexible at the picosecond timescale here studied.

SUPPORTING MATERIAL

Details of the simulation protocols and analysis, four figures, and references (58–67) are available at http://www.biophysj.org/biophysj/supplemental/S0006-3495(11)01124-6.

The authors thank Adrian H. Elcock for providing his Brownian Dynamics code and useful suggestions on simulations. We are grateful to Joe Zaccai, Jeremy C. Smith, Frank Gabel, and Pau Bernadó for valuable discussions. We thank the Galicia Supercomputing Center for computational resources.

This work was supported by grants from the Junta de Ampliación de Estudios (JAE) programme of Consejo Superior de Investigaciones Científicas, the Spanish Ministerio de Educación Ciencia (MEC) (CTQ2009-08223), and the Catalan Agency for Management of University and Research Grants (AGAUR) (2005SGR00111).

REFERENCES

1. Vieille, C., and G. J. Zeikus. 2001. Hyperthermophilic enzymes: sources, uses, and molecular mechanisms for thermostability. *Microbiol. Mol. Biol. Rev.* 65:1–43.
2. Závodszky, P., J. Kardos, …, G. A. Petsko. 1998. Adjustment of conformational flexibility is a key event in the thermal adaptation of proteins. *Proc. Natl. Acad. Sci. USA.* 95:7406–7411.
3. Hernandez, G., F. E. Jenney, Jr., …, D. M. LeMaster. 2000. Millisecond time scale conformational flexibility in a hyperthermophile protein at ambient temperature. *Proc. Natl. Acad. Sci. USA.* 97:3166–3170.
4. Fitter, J., and J. Heberle. 2000. Structural equilibrium fluctuations in mesophilic and thermophilic alpha-amylase. *Biophys. J.* 79:1629–1636.
5. Wolf-Watz, M., V. Thai, …, D. Kern. 2004. Linkage between dynamics and catalysis in a thermophilic-mesophilic enzyme pair. *Nat. Struct. Mol. Biol.* 11:945–949.
6. Butterwick, J. A., J. Patrick Loria, …, A. G. Palmer, 3rd. 2004. Multiple time scale backbone dynamics of homologous thermophilic and mesophilic ribonuclease HI enzymes. *J. Mol. Biol.* 339:855–871.
7. Salmon, L., G. Bouvignies, …, M. Blackledge. 2011. Nuclear magnetic resonance provides a quantitative description of protein conformational flexibility on physiologically important time scales. *Biochemistry.* 50:2735–2747.
8. Tehei, M., D. Madern, …, G. Zaccai. 2005. Neutron scattering reveals the dynamic basis of protein adaptation to extreme temperature. *J. Biol. Chem.* 280:40974–40979.
9. Zaccai, G. 2000. How soft is a protein? A protein dynamics force constant measured by neutron scattering. *Science.* 288:1604–1607.
10. Tehei, M., B. Franzetti, …, G. Zaccai. 2004. Adaptation to extreme environments: macromolecular dynamics in bacteria compared in vivo by neutron scattering. *EMBO Rep.* 5:66–70.
11. Tehei, M., D. Madern, …, G. Zaccai. 2001. Fast dynamics of halophilic malate dehydrogenase and BSA measured by neutron scattering under various solvent conditions influencing protein stability. *Proc. Natl. Acad. Sci. USA.* 98:14356–14361.
12. Tarek, M., and D. J. Tobias. 1999. Environmental dependence of the dynamics of protein hydration water. *J. Am. Chem. Soc.* 121:9740–9741.
13. Tarek, M., G. J. Martyna, and D. J. Tobias. 2000. Amplitudes and frequencies of protein dynamics: analysis of discrepancies between neutron scattering and molecular dynamics simulations. *J. Am. Chem. Soc.* 122:10450–10451.
14. Tarek, M., and D. J. Tobias. 2000. The dynamics of protein hydration water: a quantitative comparison of molecular dynamics simulations and neutron-scattering experiments. *Biophys. J.* 79:3244–3257.
15. Wood, K., A. Frölich, …, M. Weik. 2008. Coincidence of dynamical transitions in a soluble protein and its hydration water: direct measurements by neutron scattering and MD simulations. *J. Am. Chem. Soc.* 130:4586–4587.
16. Wood, K., S. Grudinin, …, G. Zaccai. 2008. Dynamical heterogeneity of specific amino acids in bacteriorhodopsin. *J. Mol. Biol.* 380: 581–591.
17. Wood, K., D. J. Tobias, …, M. Weik. 2010. The low-temperature inflection observed in neutron scattering measurements of proteins is due to methyl rotation: direct evidence using isotope labeling and molecular dynamics simulations. *J. Am. Chem. Soc.* 132:4990–4991.
18. McGuffee, S. R., and A. H. Elcock. 2006. Atomically detailed simulations of concentrated protein solutions: the effects of salt, pH, point mutations, and protein concentration in simulations of 1000-molecule systems. *J. Am. Chem. Soc.* 128:12098–12110.
19. McGuffee, S. R., and A. H. Elcock. 2010. Diffusion, crowding & protein stability in a dynamic molecular model of the bacterial cytoplasm. *PLOS Comput. Biol.* 6:e1000694.
20. Mereghetti, P., R. R. Gabdoulline, and R. C. Wade. 2010. Brownian dynamics simulation of protein solutions: structural and dynamical properties. *Biophys. J.* 99:3782–3791.
21. Gabel, F., D. Bicout, …, G. Zaccai. 2002. Protein dynamics studied by neutron scattering. *Q. Rev. Biophys.* 35:327–367.
22. Pérez, J., J. M. Zanotti, and D. Durand. 1999. Evolution of the internal dynamics of two globular proteins from dry powder to solution. *Biophys. J.* 77:454–469.
23. Hayward, J. A., J. L. Finney, …, J. C. Smith. 2003. Molecular dynamics decomposition of temperature-dependent elastic neutron scattering by a protein solution. *Biophys. J.* 85:679–685.
24. Gabel, F. 2005. Protein dynamics in solution and powder measured by incoherent elastic neutron scattering: the influence of Q-range and energy resolution. *Eur. Biophys. J.* 34:1–12.
25. Meinhold, L., D. Clement, …, J. C. Smith. 2008. Protein dynamics and stability: the distribution of atomic fluctuations in thermophilic and mesophilic dihydrofolate reductase derived using elastic incoherent neutron scattering. *Biophys. J.* 94:4812–4818.
26. Lee, B. I., C. Chang, …, S. W. Suh. 2001. Crystal structure of the MJ0490 gene product of the hyperthermophilic archaebacterium *Methanococcus jannaschii*, a novel member of the lactate/malate family of dehydrogenases. *J. Mol. Biol.* 307:1351–1362.
27. Dunn, C. R., H. M. Wilks, …, J. J. Holbrook. 1991. Design and synthesis of new enzymes based on the lactate dehydrogenase framework. *Philos. Trans. R. Soc. Lond. B Biol. Sci.* 332:177–184.
28. Hess, B., C. Kutzner, …, E. Lindahl. 2008. GROMACS 4: Algorithms for highly efficient, load-balanced, and scalable molecular simulation. *J. Chem. Theory Comput.* 4:435–447.
29. Hayward, J. A., and J. C. Smith. 2002. Temperature dependence of protein dynamics: computer simulation analysis of neutron scattering properties. *Biophys. J.* 82:1216–1225.
30. Róg, T., K. Murzyn, …, G. R. Kneller. 2003. nMoldyn: a program package for a neutron scattering oriented analysis of molecular dynamics simulations. *J. Comput. Chem.* 24:657–667.
31. Berendsen, H. J. C., J. P. M. Postma, …, J. R. Haak. 1984. Molecular dynamics with coupling to an external bath. *J. Chem. Phys.* 81:3684–3690.
32. Jorgensen, W. L., D. S. Maxwell, and J. Tirado-Rives. 1996. Development and testing of the OPLS all-atom force field on conformational energetics and properties of organic liquids. *J. Am. Chem. Soc.* 118:11225–11236.
33. Jorgensen, W. L., J. Chandrasekhar, …, M. L. Klein. 1983. Comparison of simple potential functions for simulating liquid water. *J. Chem. Phys.* 79:926–935.
34. Darden, T., D. York, and L. Pedersen. 1993. Particle mesh Ewald - an N·log(N) method for Ewald sums in large systems. *J. Chem. Phys.* 98:10089–10092.
35. Hess, B., H. Bekker, …, J. Fraaije. 1997. LINCS: A linear constraint solver for molecular simulations. *J. Comput. Chem.* 18:1463–1472.
36. Hamaneh, M. B., L. Zhang, and M. Buck. 2011. A direct coupling between global and internal motions in a single domain protein? MD Investigation of extreme scenarios. *Biophys. J.* 101:196–204.
37. Humphrey, W., A. Dalke, and K. Schulten. 1996. VMD: visual molecular dynamics. *J. Mol. Graph.* 14:33–38, 27–28.
38. Baker, N. A., D. Sept, …, J. A. McCammon. 2001. Electrostatics of nanosystems: application to microtubules and the ribosome. *Proc. Natl. Acad. Sci. USA.* 98:10037–10041.
39. Fogolari, F., A. Brigo, and H. Molinari. 2002. The Poisson-Boltzmann equation for biomolecular electrostatics: a tool for structural biology. *J. Mol. Recognit.* 15:377–392.
40. Holm, L., S. Kääriäinen, …, A. Schenkel. 2008. Searching protein structure databases with DaliLite v.3. *Bioinformatics.* 24:2780–2781.
41. Ellis, R. J. 2001. Macromolecular crowding: obvious but underappreciated. *Trends Biochem. Sci.* 26:597–604.

42. Kumar, S., and R. Nussinov. 2001. How do thermophilic proteins deal with heat? *Cell. Mol. Life Sci.* 58:1216–1233.

43. de Bakker, P. I. W., P. H. Hünenberger, and J. A. McCammon. 1999. Molecular dynamics simulations of the hyperthermophilic protein sac7d from *Sulfolobus acidocaldarius*: contribution of salt bridges to thermostability. *J. Mol. Biol.* 285:1811–1830.

44. Thomas, A. S., and A. H. Elcock. 2004. Molecular simulations suggest protein salt bridges are uniquely suited to life at high temperatures. *J. Am. Chem. Soc.* 126:2208–2214.

45. Danciulescu, C., R. Ladenstein, and L. Nilsson. 2007. Dynamic arrangement of ion pairs and individual contributions to the thermal stability of the cofactor-binding domain of glutamate dehydrogenase from *Thermotoga maritima*. *Biochemistry.* 46:8537–8549.

46. Vinther, J. M., S. M. Kristensen, and J. J. Led. 2010. Enhanced stability of a protein with increasing temperature. *J. Am. Chem. Soc.* 133: 271–278.

47. Karshikoff, A., and R. Ladenstein. 2001. Ion pairs and the thermotolerance of proteins from hyperthermophiles: a "traffic rule" for hot roads. *Trends Biochem. Sci.* 26:550–556.

48. Ando, T., and J. Skolnick. 2010. Crowding and hydrodynamic interactions likely dominate in vivo macromolecular motion. *Proc. Natl. Acad. Sci. USA.* 107:18457–18462.

49. Nucci, N. V., M. S. Pometun, and A. J. Wand. 2011. Site-resolved measurement of water-protein interactions by solution NMR. *Nat. Struct. Mol. Biol.* 18:245–249.

50. Halle, B. 2004. Protein hydration dynamics in solution: a critical survey. *Philos. Trans. R. Soc. Lond. B Biol. Sci.* 359:1207–1223, discussion 1223–1224, 1323–1328.

51. Modig, K., E. Liepinsh, …, B. Halle. 2004. Dynamics of protein and peptide hydration. *J. Am. Chem. Soc.* 126:102–114.

52. Ahmad, M., W. Gu, …, V. Helms. 2011. Adhesive water networks facilitate binding of protein interfaces. *Nat. Commun.* 2:261.

53. Halle, B., and M. Davidovic. 2003. Biomolecular hydration: from water dynamics to hydrodynamics. *Proc. Natl. Acad. Sci. USA.* 100: 12135–12140.

54. Melchionna, S., R. Sinibaldi, and G. Briganti. 2006. Explanation of the stability of thermophilic proteins based on unique micromorphology. *Biophys. J.* 90:4204–4212.

55. Sterpone, F., C. Bertonati, …, S. Melchionna. 2009. Key role of proximal water in regulating thermostable proteins. *J. Phys. Chem. B.* 113:131–137.

56. Meechai, N., A. M. Jamieson, and J. Blackwell. 1999. Translational diffusion coefficients of bovine serum albumin in aqueous solution at high ionic strength. *J. Colloid Interface Sci.* 218:167–175.

57. Roosen-Runge, F., M. Hennig, …, F. Schreiber. 2010. Protein diffusion in crowded electrolyte solutions. *Biochim. Biophys. Acta.* 1804:68–75.

58. Dolinsky, T. J., J. E. Nielsen, …, N. A. Baker. 2004. PDB2PQR: an automated pipeline for the setup of Poisson-Boltzmann electrostatics calculations. *Nucleic Acids Res.* 32(Web Server issue):W665–W667.

59. Li, H., A. D. Robertson, and J. H. Jensen. 2005. Very fast empirical prediction and rationalization of protein pK(a) values. *Proteins.* 61:704–721.

60. Gabdoulline, R. R., and R. C. Wade. 1996. Effective charges for macromolecules in solvent. *J. Phys. Chem.* 100:3868–3878.

61. Gabdoulline, R. R., and R. C. Wade. 1997. Simulation of the diffusional association of barnase and barstar. *Biophys. J.* 72:1917–1929.

62. García De La Torre, J., M. L. Huertas, and B. Carrasco. 2000. Calculation of hydrodynamic properties of globular proteins from their atomic-level structure. *Biophys. J.* 78:719–730.

63. Hinsen, K. 2000. The molecular modeling toolkit: A new approach to molecular simulations. *J. Comput. Chem.* 21:79–85.

64. Haynes, W. M., editor. 2010–2011. CRC Handbook of Chemistry and Physics, 91st Ed. CRC Press, Boca Raton, FL.

65. Madern, D., C. Ebel, …, G. Zaccai. 2001. Differences in the oligomeric states of the LDH-like L-MalDH from the hyperthermophilic archaea *Methanococcus jannaschii* and *Archaeoglobus fulgidus*. *Biochemistry.* 40:10310–10316.

66. Velev, O. D., E. W. Kaler, and A. M. Lenhoff. 1998. Protein interactions in solution characterized by light and neutron scattering: comparison of lysozyme and chymotrypsinogen. *Biophys. J.* 75:2682–2697.

67. Svergun, D. I., S. Richard, …, G. Zaccai. 1998. Protein hydration in solution: experimental observation by x-ray and neutron scattering. *Proc. Natl. Acad. Sci. USA.* 95:2267–2272.